

## ARTICLE OPEN

## Extreme wet and dry conditions affected differently by greenhouse gases and aerosols

Jana Sillmann<sup>1</sup>, Camilla W. Stjern<sup>1</sup>, Gunnar Myhre<sup>1</sup>, Bjørn H. Samset<sup>1</sup>, Øivind Hodnebrog<sup>1</sup>, Timothy Andrews<sup>2</sup>, Olivier Boucher<sup>3</sup>, Gregory Faluvegi<sup>4</sup>, Piers Forster<sup>5</sup>, Matthew R. Kasoar<sup>6,7</sup>, Viatcheslav V. Kharin<sup>8</sup>, Alf Kirkevåg<sup>9</sup>, Jean-Francois Lamarque<sup>10</sup>, Dirk J. L. Olivie<sup>9</sup>, Thomas B. Richardson<sup>11</sup>, Drew Shindell<sup>12</sup>, Toshihiko Takemura<sup>13</sup>, Apostolos Voulgarakis<sup>7</sup> and Francis W. Zwiers<sup>14</sup>

Global warming due to greenhouse gases and atmospheric aerosols alter precipitation rates, but the influence on extreme precipitation by aerosols relative to greenhouse gases is still not well known. Here we use the simulations from the Precipitation Driver and Response Model Intercomparison Project that enable us to compare changes in mean and extreme precipitation due to greenhouse gases with those due to black carbon and sulfate aerosols, using indicators for dry extremes as well as for moderate and very extreme precipitation. Generally, we find that the more extreme a precipitation event is, the more pronounced is its response relative to global mean surface temperature change, both for aerosol and greenhouse gas changes. Black carbon (BC) stands out with distinct behavior and large differences between individual models. Dry days become more frequent with BC-induced warming compared to greenhouse gases, but so does the intensity and frequency of extreme precipitation. An increase in sulfate aerosols cools the surface and thereby the atmosphere, and thus induces a reduction in precipitation with a stronger effect on extreme than on mean precipitation. A better understanding and representation of these processes in models will provide knowledge for developing strategies for both climate change and air pollution mitigation.

*npj Climate and Atmospheric Science* (2019)2:24; <https://doi.org/10.1038/s41612-019-0079-3>

## INTRODUCTION

Under global warming, the amount of extreme precipitation is expected to increase about three times as much as mean precipitation, with distinct regional patterns (e.g., see refs <sup>1,2</sup>). Observations also show that heavy precipitation increases more than the mean precipitation.<sup>3,4</sup> While recent studies emphasized the robustness of the projected changes in precipitation extremes on large-aggregated scales, our understanding of regional to local changes in precipitation extremes remains limited.<sup>5</sup> Various dynamic and thermodynamic mechanisms influence the regional patterns of changes in extreme precipitation,<sup>6–9</sup> on short and long time scales.<sup>10,11</sup>

Energy balance studies clearly show that aerosols differ from greenhouse gases in their impact on precipitation.<sup>12–15</sup> Unlike greenhouse gases, atmospheric aerosols also responsible for air pollution are not distributed homogeneously around the globe, but have distinct regional distributions.<sup>16</sup> Especially, regions with high emissions from fossil fuel burning sources (e.g. power plants, traffic), such as South Asia, exhibit high concentrations of sulfate and black carbon (BC).<sup>17</sup> Through long-range transport,<sup>18</sup> these emissions can also affect remote regions, such as the Arctic.

Atmospheric aerosols are suggested to impact precipitation in various ways, such as by influencing large-scale circulation and changes in the intertropical convergence zone<sup>19–21</sup> through general cooling of the surface,<sup>22–24</sup> by changing atmospheric stability,<sup>22,25–27</sup> and by influencing cloud microphysics.<sup>28–30</sup> Moreover, scattering aerosols, such as sulfate, may influence these processes in different ways than absorbing aerosols, such as BC. The global mean precipitation change is constrained by the energy budget,<sup>6,31,32</sup> whereas there seems to be no such constraint on the global change in extreme precipitation. In addition, the effect of inhomogeneous aerosol burdens in the atmosphere and varying circulation adjustments can lead to regionally diversified patterns of changes in mean and extreme precipitation (e.g., see refs <sup>33–36</sup>).

Precipitation change occurs both as fast response to a change in greenhouse gas or aerosol concentrations, through short timescale alterations to stability and the atmospheric energy balance, and on longer time scales, through changes in mean surface temperature.<sup>22,27,37,38</sup> The fast global mean precipitation change scales strongly with absorption of radiation in the atmospheric column and the slow response (feedback driven)

<sup>1</sup>Center for International Climate Research—Oslo, Gaustadalléen 21, 0349 Oslo, Norway; <sup>2</sup>Met Office Hadley Centre, FitzRoy Road, Exeter EX1 3PB, UK; <sup>3</sup>Institut Pierre-Simon Laplace, Sorbonne Université, CNRS, 3 Rue Michel Ange, 75016 Paris, France; <sup>4</sup>NASA Goddard Institute for Space Studies and Center for Climate Systems Research, Columbia University, New York, NY 10025, USA; <sup>5</sup>Priestley International Centre for Climate University of Leeds, Leeds LS2 9JT, UK; <sup>6</sup>Grantham Institute—Climate Change and the Environment, Imperial College London, London, UK; <sup>7</sup>Department of Physics, Imperial College London, Prince Consort Rd, Kensington, London SW7 2BB, UK; <sup>8</sup>Canadian Center for Climate Modelling and Analysis, Climate Research Division, Environment and Climate Change Canada, University of Victoria, PO Box 1700 STN CSC, Victoria, BC V8W 2Y2, Canada; <sup>9</sup>Norwegian Meteorological Institute, P.O. Box 43 Blindern, 0313 Oslo, Norway; <sup>10</sup>National Center for Atmospheric Research, P.O. Box 3000, Boulder, CO 80305, USA; <sup>11</sup>School of Earth and Environment, University of Leeds, Leeds, UK; <sup>12</sup>Nicholas School of the Environment, Duke University, Durham, NC 27708, USA; <sup>13</sup>Research Institute for Applied Mechanics, Kyushu University, 6-1 Kasuga-koen, Kasuga, Fukuoka 816-8580, Japan and <sup>14</sup>Pacific Climate Impacts Consortium, University House 1, University of Victoria, PO Box 1700Stn CSC, Victoria, BC V8W 2Y2, Canada

Correspondence: Jana Sillmann (jana.sillmann@cicero.oslo.no)

Received: 5 September 2018 Accepted: 13 June 2019

Published online: 17 July 2019

scales with global surface temperature change.<sup>22,24,26</sup> How different drivers of climate change, such as greenhouse gases and aerosols, impact extreme precipitation is currently highly uncertain both on global and regional scales. Studies indicate that changes in extreme precipitation are driven by the surface temperature change, thus being independent from the forcing mechanism.<sup>5,39</sup> However, Lin et al.<sup>40</sup> and Wang et al.<sup>41</sup> find indications of driver dependency for more moderate extreme precipitation. This indicates that results depend on what exact definition of extreme precipitation is used for the analyses, as outlined also in Sillmann et al.<sup>42</sup>

We find in this study, that the more extreme a precipitation event is, the more pronounced is its response relative to global mean surface temperature change, both for aerosol and greenhouse gas changes. With BC-induced warming dry days become more frequent, but also the intensity and frequency of extreme precipitation increases. Sulfate aerosols cause a cooling of the atmosphere, and thus induces a reduction in precipitation with a stronger effect on extreme than on mean precipitation.

## RESULTS AND DISCUSSION

Using the model simulations from the Precipitation Driver and Response Model Intercomparison Project (PDRMIP),<sup>43</sup> we are able to investigate in more detail the responses of mean and extreme precipitation to different climate forcing agents. Experiments were run for globally increased levels of carbon dioxide ( $\text{CO}_2 \times 2$ ), methane ( $\text{CH}_4 \times 3$ ), sulfate ( $\text{SO}_4 \times 5$ ), BC ( $\text{BC} \times 10$ ), and solar forcing (SOL) compared to baseline experiments representing present-day conditions using aerosol concentrations from AeroCom Phase II.<sup>44,45</sup> For more details on the experiments and models see “Methods”.

To assess extreme precipitation, we calculate the annual maximum 1-day precipitation amount (Rx1day), which occurs by definition once every year and resembles approximately the 99.7th percentile of the daily precipitation distribution. In addition, to capture events that are much more extreme, we use the 99.99th percentile of the daily precipitation distribution, which is expected to occur only every 30 years. Extreme precipitation changes more than mean precipitation, when calculated as a relative change in precipitation per degree increase in global

mean surface temperature ( $\Delta T$ ) for increased  $\text{CO}_2$  forcing (see Fig. 7.21 in Boucher et al.,<sup>46</sup>). We extend this analysis to all the forcing agents considered in PDRMIP and show, in agreement with previous studies,<sup>24</sup> that the climate forcing mechanism plays a role for the changes seen in the mean precipitation. To allow comparison between the experiments, which represent perturbations of different scales, all figures show changes normalized by the magnitude (the absolute value) of the global mean surface temperature change for each model and experiment. This approach makes the magnitude of the responses comparable, while retaining the sign of the change expected from perturbations that cool ( $\text{SO}_4$ ) versus perturbations that warm (the other forcing agents) the climate. We provide non-normalized model mean changes in Supplementary Table 1 for reference.

The smallest mean precipitation change in the multimodel median is found for  $\text{CO}_2$ , followed by  $\text{CH}_4$ , and SOL, while the largest change occurs for sulfate aerosols, with only a small intermodel spread (Fig. 1). The tendency of sulfate to induce strongest changes (a reduction) to mean precipitation is true for all the regions considered in Fig. 1 (global and extratropical land) and Supplementary Fig. 1 (ocean, land, and tropical land), and is related to its strong effect on the hydrological sensitivity (see also Samset et al.<sup>16</sup>). Despite producing a positive global mean temperature change, BC forcing generally reduces the mean precipitation, due to its strong influence on atmospheric absorption, which generally stabilizes the atmosphere and dampens precipitation formation (see refs<sup>12,47</sup>). There is, however, a large spread amongst the models, of which two show no change or a slight increase.

In general, as opposed to the mean precipitation, the magnitude of the change in extreme precipitation (Rx1day and the 99.99th percentile) is similar across all forcing agents with the multimodel median changes being very close to each other. Note, for instance, that the global change in the 99.99th percentile is around  $6\%/|K|$  for  $\text{CO}_2$ ,  $\text{CH}_4$ , and SOL and around  $-6\%/|K|$  for  $\text{SO}_4$ , which cools the climate and therefore reduces both mean and extreme precipitation. The intermodel spread is however large compared to mean precipitation. BC stands out with somewhat weaker changes in the extremes and with a substantially larger intermodel spread, with some models even indicating a decrease in extreme precipitation. Over extratropical land (i.e. latitudes

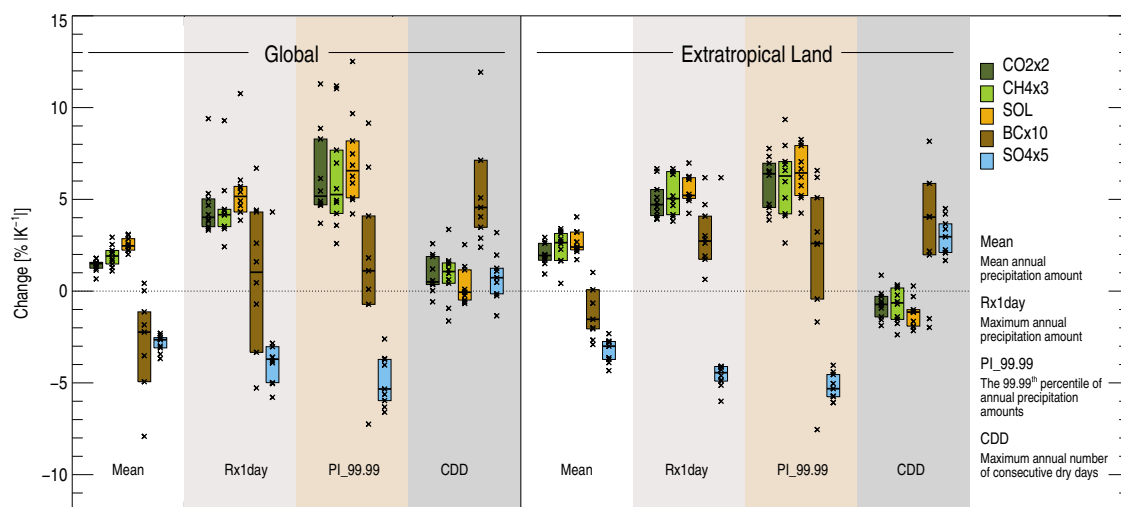


**Fig. 1** Relative changes in mean precipitation and dry and wet extremes for the different forcing agents. All values are defined and calculated for each grid box, regionally averaged for baseline and perturbed climate, before relative changes are calculated. These changes are then normalized by the absolute value of the global mean temperature change. Extreme precipitation is expressed in terms of the annual maximum 1-day precipitation amount (Rx1day) and in terms of the precipitation intensity of the upper 99.99th percentile of daily precipitation (PI\_99.99), and extreme dry conditions in terms of the annual number of consecutive dry days (CDD). Box sizes show the interquartile range, the model median is shown as a solid line, and crosses indicate individual model values

polewards of 30°S and 30°N), all models agree that the intensity of the annual maximum precipitation (Rx1day) increases for all forcing agents except sulfate (see Supplementary Fig. 1 for changes over oceans, global land, and tropical land). Globally, the change in extreme precipitation is for all forcing agents generally larger for the intensity of the 99.99th percentile (PI<sub>99.99</sub>) than for Rx1day supporting earlier findings<sup>3,5</sup> (Fig. 1). The multimodel median difference between the change in very extreme precipitation (99.99th percentile) and the change in Rx1day is smallest for SO<sub>4</sub> (see Supplementary Fig. 2). Further research based on more model simulations, and ideally observations, is needed to understand the changes in extreme precipitation associated with sulfate forcing, particularly for very extreme precipitation, as sampling uncertainties are very large.

We find the same type of response for the frequency of precipitation events with different intensities. Supplementary Fig. 3 shows that the more intense the precipitation event (i.e., higher percentiles), the larger the relative change in how often it occurs. Again, the increase (with higher precipitation intensity) in the magnitude of the change is smaller for BC and SO<sub>4</sub>. This feature is clearest for the SO<sub>4</sub> case, for which the model spread is also smaller than for BC. Also, the change for SO<sub>4</sub> in the lowermost panel, showing changes in the frequency of days with very intense precipitation (amounts above the 99.99th percentile for each given grid cell), stands out with a very small change compared to the other climate forcings. This could be due to the fact that SO<sub>4</sub> unlike the other climate forcings cools the climate, and this cooling will not necessarily induce a similar response as a warming of the same magnitude. However, caution is needed as differences in frequency in the highest percentile are very uncertain due to a very small sample size.

Due to its large effect on atmospheric absorption, BC causes a strong reduction in the fast precipitation change,<sup>24</sup> and therefore imposes a different effect on the changes in mean and extreme precipitation than the other forcing agents. At the same time, the spread between models is largest for BC, with some models showing opposite signs of change. This tendency of BC-induced climate signals to be associated with larger model spreads than those induced by other drivers is a well documented feature of the PDRMIP data set,<sup>18</sup> and is partly related to differences in experiment setups and partly to model differences in BC lifetime, absorptivity, and baseline cloud cover. For the BC and CH<sub>4</sub> perturbations, the surface temperature response is much smaller than for the other forcing agents (see Supplementary Table 1), and especially for the BC experiment some models yield a particularly weak temperature response (see inset bar plots in Fig. 3). This causes artificially strong changes in precipitation when normalized by temperature change for those models, and contributes to a particularly large model spread for BC. Overall, this uncertainty adds to the uncertainty coming from sampling very extreme events (i.e. the 99.99th percentile).

In general, BC tends to have a drying effect on mean precipitation and induces an overall smaller increase in extreme precipitation than the other forcing agents. The difference between mean and extreme precipitation response is stronger for Rx1day compared to the other climate drivers investigate here, and becomes less obvious for higher percentiles (see also Supplementary Fig. 3, and Fig. 2a for spatial patterns of Rx1day). To investigate further the drying effect of BC, we have analyzed the annual maximum number of consecutive dry days (CDD) (see Fig. 1). The increase in CDD per degree warming is largest for BC for the globe and extratropical land, although showing a large spread among the models. For extratropical land areas, BC and SO<sub>4</sub> are the only forcing agents inducing a drying trend with model median changes significantly different (at the 95% level, by the Wilcoxon signed-rank test) from zero. When looking at all land areas including the tropics, the drying effect of BC seems less pronounced compared to the other forcing agents and SO<sub>4</sub> causes

reduced CDD here (see Supplementary Fig. 1). Over tropical land, two of the models, CESM-CAM5 and MIROC-SPRINTARS, appear as extreme positive and negative outliers, respectively, as they are normalized by a warming for the BC perturbation that is close to zero. This contributes to a very large spread among the models. Despite that spread, and unlike over extratropical land, over tropical land there is more agreement about the sign of the CDD change among forcing agents, as all but SO<sub>4</sub> induce a drying. Over extratropical land, SO<sub>4</sub> shows a drying trend with a similarly large magnitude as BC, but with less spread between the models.

The regional patterns for changes in CDD per degree warming due to increase in CO<sub>2</sub>, CH<sub>4</sub>, and SOL are similar as depicted in Fig. 2b, with global spatial (Pearsons) correlation coefficients of 0.78 and 0.92. Regions with strong increases in CDD are Central America, Southern Europe, Southern Africa, and the Eastern Indian Ocean, and all induce reductions in CDD at higher northern and southern latitudes. SO<sub>4</sub> displays similar patterns but of opposite sign, while BC influences CDD in the same regions as the other drivers, but with a magnitude that is substantially higher. This pattern of strong BC-induced drying is similar to what has been found for mean precipitation change due to BC increase in another study.<sup>45</sup> Note, for example, the very strong increases over Europe/Western Russia. This difference in magnitude seems to be the main cause of the positive extratropical-average CDD change for BC (Fig. 1), contrasting the negative change for the other warming drivers CO<sub>2</sub>, CH<sub>4</sub>, and SOL (see also a corresponding figure of the annual number of dry days in Supplementary Fig. 4, which displays the same tendency). In fact, the spatial correlation between CO<sub>2</sub>- and BC-induced changes to CDD for extratropical land regions is 0.81 and highly significant. On the other hand, although the tropical average CDD changes in Supplementary Fig. 1 are similar between all warming drivers including BC, spatial correlations over tropical land masses are poorer than it was over the extratropics (i.e., 0.55 between CO<sub>2</sub> and BC). This pattern of BC-induced drying is similar to what has been found for mean precipitation change due to BC increase in another study.<sup>45</sup>

So far, we have shown that extremes of various intensities have different responses to climate forcing. In Fig. 3, we show how the frequency of different precipitation events varies for different precipitation amounts for individual models. These are absolute changes not normalized by the temperature change, which is shown for each model as bars in the Fig. 3 inset. The spread between models increases the more extreme precipitation gets, and there is also an increase in the relative intermodel standard deviation (that is, the standard deviation relative to the model mean magnitude of the change at the given precipitation intensity) for CO<sub>2</sub>, CH<sub>4</sub>, and SOL. BC has the weakest globally averaged temperature response with respect to forcing, but produces some of the strongest precipitation reductions despite increasing global mean temperature due to its strong atmospheric shortwave absorption.<sup>24,43</sup> However, it has to be noted that for the models with the weakest temperature responses (CESM-CAM5 and MIROC-SPRINTARS), the precipitation change induced by CH<sub>4</sub> and BC is within the range of natural variability even for the most intense precipitation (see Fig. 3). For the other forcing agents, the change in frequency increases (except SO<sub>4</sub>, for which it decreases) with precipitation intensity, and the signal falls well outside the range of natural variability.

For the total change in global precipitation per degree temperature change (Fig. 4 upper panel) all the warming forcing agents cause a decrease in the frequency of precipitation events with intensities up to about 5 mm/day. This is consistent with the fact that the frequency of precipitation events of intensities between 1 mm/day and the 90th percentile are reduced for these forcings (see also Supplementary Fig. 3). However, a clear distinction between aerosols and the other forcing agents can be seen over extratropical land (Fig. 4 upper right panel), where all

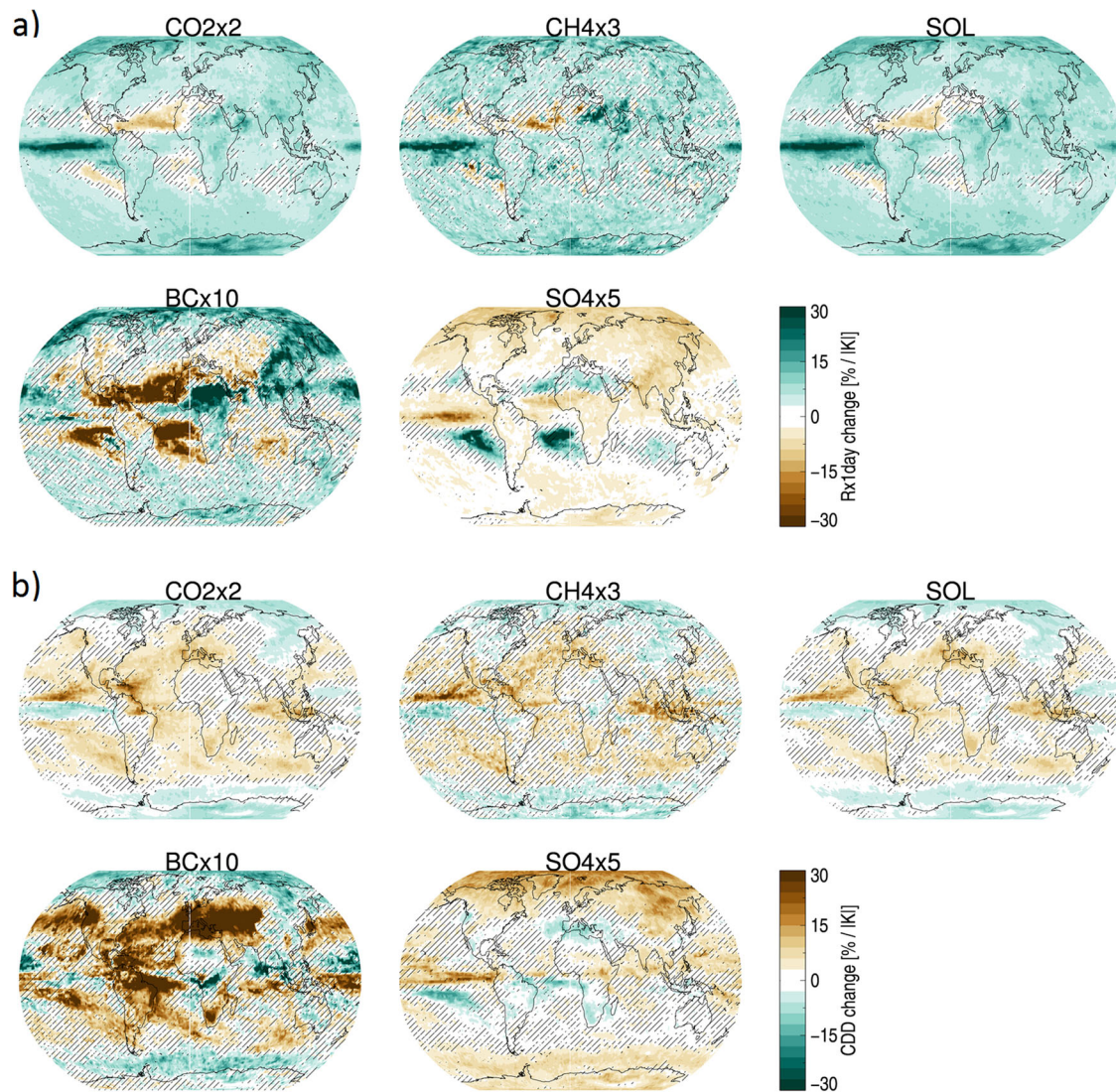


**Fig. 2** Spatial patterns of model mean changes in wet and dry extremes. Wet extremes shown in **a** as annual maximum 1-day precipitation amount (Rx1day) and dry extremes shown in **b** as number of consecutive dry days (CDD) are normalized by the absolute value of the global temperature change. Hatched areas indicate grid cells where less than 75% of the models agree on the sign of the change

except BC and  $\text{SO}_4$  lead to an increase also in the lowest precipitation amounts (up to around 30 mm/d).

Finally, precipitation changes can be disentangled into fast precipitation changes (instantaneous radiative perturbation and rapid adjustment) and feedback response (slow changes scaling with global temperature change).  $\text{CO}_2$  and SOL impose somewhat different fast precipitation changes signals in the mean precipitation, but are similar for extreme precipitation.<sup>42</sup> Earlier studies have also emphasized the particular role of BC relative to GHGs in the fast precipitation contribution to the mean precipitation change.<sup>22,24</sup> We find that for all drivers except BC, most of the total precipitation change originates from the slow feedback response (Fig. 4, middle panel), which is in a similar range as the total change (Fig. 4, upper panel). The globally averaged rapid adjustment (Fig. 4, lower panel) is generally of opposite sign and smaller in magnitude than the slow feedback response, but for BC the rapid adjustments dominate the total change for the low to medium precipitation amounts (about 40 mm/day). This could also be the cause for the difference in BC- and GHG-response in more moderate precipitation percentiles (up to the 99th percentile) as seen in Supplementary Fig. 3. However, the latter shows also that for the most extreme precipitation

percentiles (>99th percentile), the difference between the responses to aerosols and greenhouse gases diminishes, except for  $\text{SO}_4$ .

Over extratropical land, a similar transition is visible in the fast precipitation response (Fig. 4). For precipitation intensities up to about 70 mm/day, there are large differences between BC and the other forcing agents inducing a warming. While for the highest intensities, the precipitation response from BC perturbations approaches that from greenhouse gas perturbations, confirming also results from Pendergrass et al.<sup>39</sup> and Sillmann et al.<sup>42</sup> that the most extreme precipitation is independent of the type of forcing agent.

In conclusion, the PDRMIP simulations made it possible to separate the thermodynamic effect of different forcing agents on changes in mean and extreme precipitation. BC and sulfate aerosols seem to have opposing effects on extreme precipitation per absolute temperature change (see also Ocko et al.<sup>48</sup>). Sulfate aerosols, by cooling the surface, reduce both mean and extreme precipitation unlike the other forcing agents, but also increase CDD particularly in extratropical land areas. BC induces a decrease in mean precipitation despite warming the surface. Although its influence on extreme precipitation is much more uncertain due to

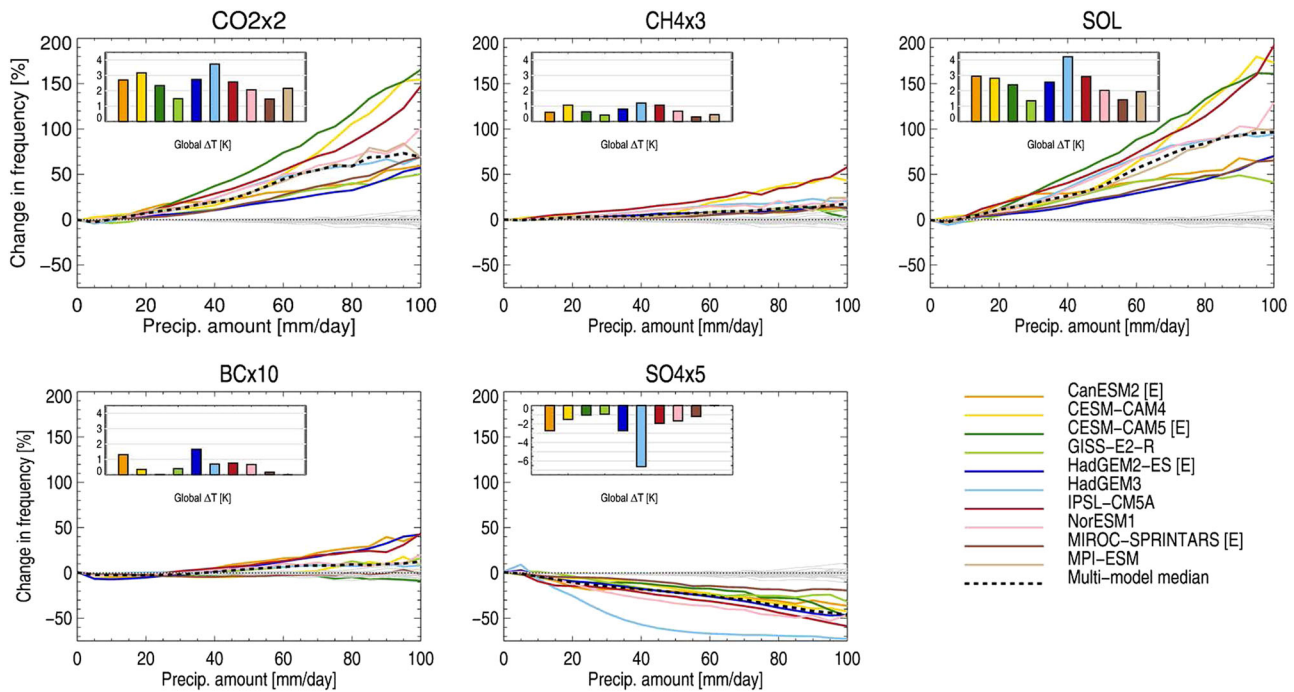


**Fig. 3** Relative changes in the frequency of different precipitation amounts for individual models and forcing agents. Note that here, the changes are not normalized by the magnitude of the global temperature change  $\Delta T$ , which instead is provided in the barplot insets in each figure panel. Gray lines show “background” variation (based on the years 1–100 of the BASE simulations) calculated from Monte Carlo simulations, as an indication of natural variability

a large model spread, all but one model simulate more positive changes in the extremes than in the mean, and over extratropical land all models predict an increase in Rx1day. BC also has the largest model spread in CDD changes. The response to BC forcing may be a significant contributor to the uncertainty in estimates of future changes in both wet and dry extremes.<sup>18,24,43</sup> This study underlines the need to improve the understanding of climate models’ responses to aerosols (along with improving global aerosol monitoring networks), for realistic projections of mean and extreme precipitation. While other PDRMIP experiments with more distinct regional aerosol forcing can provide further insights into regional climate change and air pollution mitigation,<sup>49</sup> we highlight here the differences in mean and extreme precipitation response based on globally increased sulfate and BC concentration.

## METHODS

### Precipitation Driver and Response Multimodel Intercomparison Project

In PDRMIP, ten global climate models performed baseline simulations with present-day concentrations of greenhouse gases and aerosols, and five perturbation experiments involving, respectively, a doubling of  $\text{CO}_2$  ( $\text{CO}_2 \times 2$ ), a tripling of  $\text{CH}_4$  ( $\text{CH}_4 \times 3$ ), a 2% increase in the solar constant (SOL), a tenfold increase in BC ( $\text{BC} \times 10$ ) and a fivefold increase in sulfate ( $\text{SO}_4 \times 5$ ). Note that the magnitude of the perturbations is somewhat arbitrary, but the applied perturbations were chosen to obtain robust signals in the models, and not to represent realistic past or possible future changes. Therefore, we refer only to climate responses normalized by the global mean surface temperature change that the perturbation causes, to make the experiments comparable. Both baseline and perturbation experiments were run both in a fully coupled mode, as well as in a fixed-sea surface temperature (fixed-SST) mode. The coupled simulations were run for at least 100 years and the fixed-SST simulations for at least 15 years. Analyses in the present paper are based on years 51–100 of the coupled runs and years 6–15 of the fixed-SST runs. Results from the fixed-SST simulations give us the rapid response (the fast precipitation changes, occurring within

days to weeks after the start of the perturbation), while the feedback response (the slow change, occurring within months to years after the start of the perturbations) is found by subtracting the fixed-SST response from the result of the fully coupled simulations. The reader can refer to Myhre et al.<sup>43</sup> for a more comprehensive description of the experiments and the models used.

### Averaged precipitation extremes

For each model and grid cell, we calculate the mean precipitation, Rx1day (i.e., the annual maximum 1-day precipitation amount) and the 99.99th percentile—first averaged overall daily values from the last 50 years of the BASE simulation, and then averaged over the same years for the five perturbation simulations (the cases). The relative difference between the globally averaged values of, for instance, Rx1day for BASE and each case are then calculated and divided by global mean surface temperature change for the given model and case. The state-of-the-art models as used in the PDRMIP experiments have been previously assessed with regard to their ability to simulate mean and extreme precipitation.<sup>2</sup>

### Histograms

To calculate histograms of relative changes in occurrence for fixed 5-mm/day precipitation intervals, we count how often precipitation falls within a given intensity interval for each grid cell, model, and for BASE as well as the five forcing agents. We use daily values for the last 50 years of the coupled simulations and normalize this number by the number of available data points. This gives, for each grid cell, a number between 0 and 1 (the frequency of occurrence), depending on how often precipitation of that intensity occurs. We then, for each model and case, calculate the percent change in the globally averaged frequency of occurrence, divided by the global mean surface temperature change for the given model and case. Note, however, that the fast changes were not divided by the global temperature changes in the end, as these do not scale with the applied radiative forcing.

### Natural variability

To provide an estimate of how much signals in Fig. 4 deviate from natural variability, we utilize all available years in the BASE runs (around 100 years,

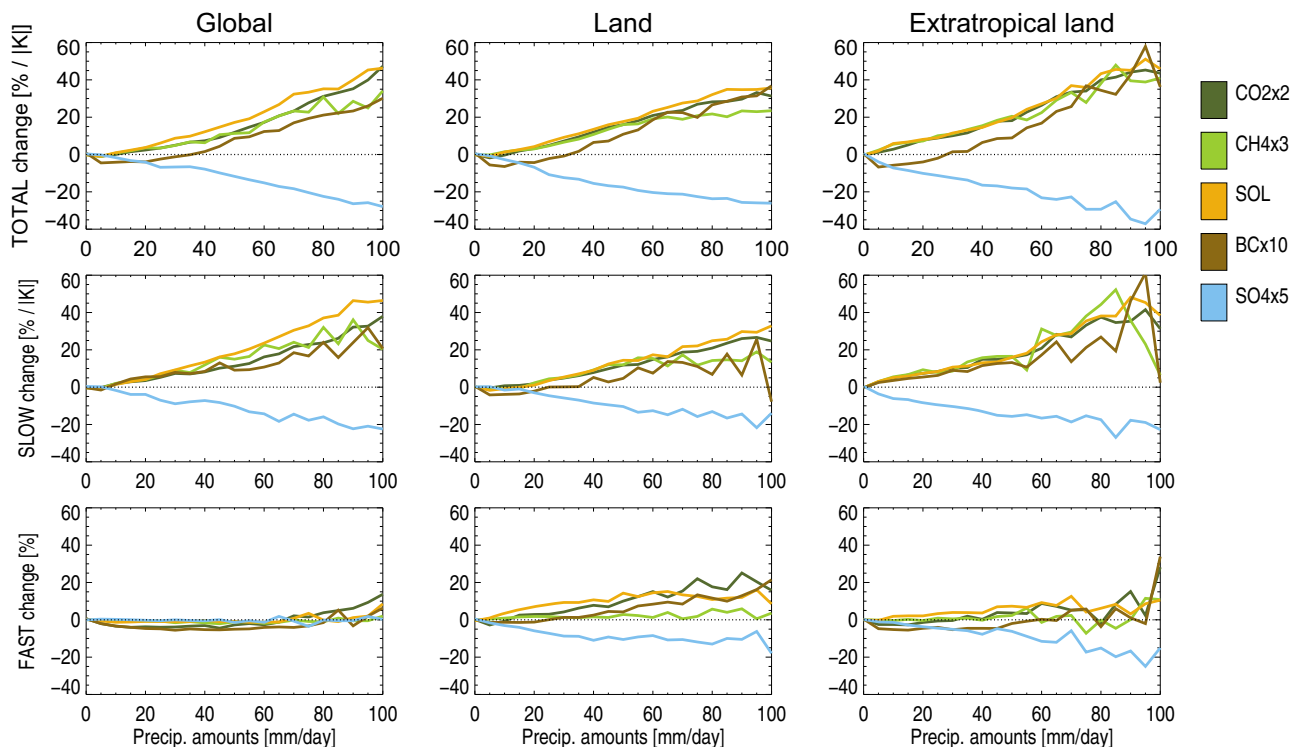


**Fig. 4** Relative changes in the total, fast, and slow response of different precipitation amounts. Changes are separated in total (upper panel), slow (middle panel), and fast responses (lower panel) of precipitation due to different forcing agents for different precipitation amounts averaged over the globe, global land, and extratropical land (poleward of 30°N or S) regions, using a bin size of 5 mm/day. Note that for the total and slow responses, quantities are normalized by the absolute value of the global mean surface temperature change for the given case. For the fast response such normalization cannot be performed since it is quantified by using simulations keeping the sea surface temperature fixed

varying slightly between models). We construct a precipitation series based on random picks from the entire time series, and then count the frequency of occurrence in each precipitation bin for this random precipitation time series, as well as the difference relative to the “original” BASE used in the analyses above. This procedure is repeated ten times, and the largest positive and negative difference from the original BASE for each bin is then plotted as a gray line in Fig. 3, together with individual model changes. As there is no temperature change in BASE, we do not normalize by global mean temperature change in Fig. 3.

## DATA AVAILABILITY

All PDRMIP model results used for the present study are available to the public through the Norwegian FEIDE data storage facility. The datasets used for the figures are available upon request from the corresponding author. For more information, see [www.cicero.uio.no/en/PDRMIP](http://www.cicero.uio.no/en/PDRMIP).

## CODE AVAILABILITY

Analysis code is available upon request from the corresponding author. For climate model code, refer to the respective authors of the references cited in Table 3 in Myhre et al.<sup>43</sup>

## ACKNOWLEDGEMENTS

O.B. acknowledges HPC resources from TGCC under the gencomp6 allocation provided by GENCI (Grand Equipement National de Calcul Intensif). J.S., C.W.S., G.M., Ø.H., and B.H.S. are supported by the projects NAPEX (grant no. 229778) and SUPER (grant no. 250573) funded by the Norwegian Research Council. T.A. was supported by the Met Office Hadley Centre Climate Programme funded by BEIS and Defra. A.V. and M.R.K. were supported by the Natural Environment Research Council (grant NE/K500872/1). T.B.R. was supported by a NERC CASE award NE/K007483/1 in collaboration with the Met Office and NERC grant NE/N006038/1. Simulations with

HadGEM3-GA4 were performed using the MONSooN system, a collaborative facility supplied under the Joint Weather and Climate Research Programme, which is a strategic partnership between the Met Office and the Natural Environment Research Council. Climate modeling at GISS is supported by the NASA Modeling, Analysis and Prediction program. GISS simulations used resources provided by the NASA High-End Computing Program through the NASA Center for Climate Simulation at Goddard Space Flight Center.

## AUTHOR CONTRIBUTIONS

J.S., G.M., B.H.S. and Ø.H. designed the study, C.W.S. did the analysis, and J.S. and C.W.S. wrote the manuscript. B.H.S., T.A., O.B., G.F., P.F., M.R.K., V.V.K., A.K., J.F.L., D.J.L.O., T.B.R., D.S., T.T. and A.V. contributed with model simulations. All authors contributed to the discussion of the results and revised the text critically for important intellectual content. All authors gave final approval of the completed version. J.S. is ensuring that questions related to the accuracy or integrity of any part of the work are appropriately investigated and resolved.

## ADDITIONAL INFORMATION

**Supplementary information** accompanies the paper on the *npj Climate and Atmospheric Science* website (<https://doi.org/10.1038/s41612-019-0079-3>).

**Competing interests:** The authors declare no competing interests.

**Publisher's note:** Springer Nature remains neutral with regard to jurisdictional claims in published maps and institutional affiliations.

## REFERENCES

1. Kharin, V. V., Zwiers, F. W., Zhang, X. & Wehner, M. Changes in temperature and precipitation extremes in the CMIP5 ensemble. *Clim. Change*. **119**, 345–357 (2013).

2. Sillmann, J., Kharin, V. V., Zhang, X., Zwiers, F. W. & Bronaugh, D. Climate extremes indices in the CMIP5 multimodel ensemble: Part 1. Model evaluation in the present climate. *J. Geophys. Res.* **118**, 1716–1733 (2013).
3. Donat, M. G., Lowry, A. L., Alexander, L. V., Ogorman, P. A. & Maher, N. More extreme precipitation in the world's dry and wet regions. *Nat. Clim. Change* **6**, 508–513 (2016).
4. Fischer, E. M. & Knutti, R. Observed heavy precipitation increase confirms theory and early models. *Nat. Clim. Change* **6**, 986–991 (2016).
5. Fischer, E. M., Beyerle, U. & Knutti, R. Robust spatially aggregated projections of climate extremes. *Nat. Clim. Change* **3**, 1033–1038 (2013).
6. Allen, M. R. & Ingram, W. J. Constraints on future changes in climate and the hydrologic cycle. *Nature* **419**, 224–232 (2002).
7. O'Gorman, P. A. Precipitation extremes under climate change. *Curr. Clim. Change Rep.* **1**, 49–59 (2015).
8. Trenberth, K. E. Conceptual Framework for Changes of Extremes of the Hydrological Cycle with Climate Change. *Clim. Change* **42**, 327–339 (1999).
9. Pfahl, S., O'Gorman, P. A. & Fischer, E. M. Understanding the regional pattern of projected future changes in extreme precipitation. *Nat. Clim. Change* **7**, 423–427 (2017).
10. Westra, S. et al. Future changes to the intensity and frequency of short-duration extreme rainfall. *Rev. Geophys.* **52**, 522–555 (2014).
11. Prein, A. F. et al. The future intensification of hourly precipitation extremes. *Nat. Clim. Change* **7**, 48–52 (2016).
12. Richardson, T. et al. Drivers of precipitation change: an energetic understanding. *J. Clim.* **31**, 9641–9657 (2017).
13. Hodnebrog, O., Myhre, G., Forster, P. M., Sillmann, J. & Samset, B. H. Local biomass burning is a dominant cause of the observed precipitation reduction in southern Africa. *Nat. Commun.* **7**, 11236 (2016).
14. O'Gorman, P., Allan, R., Byrne, M. & Previdi, M. Energetic constraints on precipitation under climate change. *Surv. Geophys.* **33**, 585–608 (2012).
15. Pendergrass, A. G. & Hartmann, D. L. The atmospheric energy constraint on global-mean precipitation change. *J. Clim.* **27**, 757–768 (2014).
16. Samset, B. H. et al. Climate impacts from a removal of anthropogenic aerosol emissions. *Geophys. Res. Lett.* **45**, 1020–1029 (2018).
17. Hoelsy, R. M. et al. Historical (1750–2014) anthropogenic emissions of reactive gases and aerosols from the Community Emission Data System (CEDS). *Geosci. Model Dev.* **2017**, 1–41 (2017).
18. Stjern, C. W. et al. Rapid adjustments cause weak surface temperature response to increased black carbon concentrations. *J. Geophys. Res.* **122**, 11,462–411,481 (2017).
19. Iles, C. E. & Hegerl, G. C. The global precipitation response to volcanic eruptions in the CMIP5 models. *Environ. Res. Lett.* **9**, 104012 (2014).
20. Haywood, J. M., Jones, A., Bellouin, N. & Stephenson, D. Asymmetric forcing from stratospheric aerosols impacts Sahelian rainfall. *Nat. Clim. Change* **3**, 660–665 (2013).
21. Hwang, Y.-T., Frierson, D. M. W. & Kang, S. M. Anthropogenic sulfate aerosol and the southward shift of tropical precipitation in the late 20th century. *Geophys. Res. Lett.* **40**, 2845–2850 (2013).
22. Andrews, T., Forster, P. M., Boucher, O., Bellouin, N. & Jones, A. Precipitation, radiative forcing and global temperature change. *Geophys. Res. Lett.* **37**, L14701 (2010).
23. Baker, L. H. et al. Climate responses to anthropogenic emissions of short-lived climate pollutants. *Atmos. Chem. Phys.* **15**, 8201–8216 (2015).
24. Samset, B. H. et al. Fast and slow precipitation responses to individual climate forcings: a PDRMIP multimodel study. *Geophys. Res. Lett.* **43**, 2782–2791 (2016).
25. Ban-Weiss, G. A., Cao, L., Bala, G. & Caldeira, K. Dependence of climate forcing and response on the altitude of black carbon aerosols. *Clim. Dyn.* **38**, 897–911 (2011).
26. Kvalevåg, M. M., Samset, B. H. & Myhre, G. Hydrological sensitivity to greenhouse gases and aerosols in a global climate model. *Geophys. Res. Lett.* **40**, 1432–1438 (2013).
27. Ming, Y., Ramaswamy, V. & Persad, G. Two opposing effects of absorbing aerosols on global-mean precipitation. *Geophys. Res. Lett.* **37**, L13701 (2010).
28. Feingold, G., Cotton, W., Lohmann, U. & Levin, Z. Effects of pollution aerosol and biomass burning on clouds and precipitation: numerical modeling studies. In *Aerosol Pollution Impact on Precipitation*. (eds Levin, Z. & Cotton, W. R.) 243–276 (Springer, Dordrecht, 2009).
29. Koren, I. et al. Aerosol-induced intensification of rain from the tropics to the mid-latitudes. *Nat. Geosci.* **5**, 118–122 (2012).
30. Rosenfeld, D. et al. Aerosol effects on microstructure and intensity of tropical cyclones. *Bull. Am. Meteor. Soc.* **93**, 987–1001 (2012).
31. Mitchell, J. F. B., Wilson, C. A. & Cunningham, W. M. On CO<sub>2</sub> climate sensitivity and model dependence of results. *Q. J. R. Meteorol. Soc.* **113**, 293–322 (1987).
32. Thackeray, C. W., DeAngelis, A. M., Hall, A., Swain, D. L. & Qu, X. On the connection between global hydrologic sensitivity and regional wet extremes. *Geophys. Res. Lett.* **45**, 11,343–11,351 (2018).
33. Pall, P., Allen, M. R. & Stone, D. A. Testing the Clausius–Clapeyron constraint on changes in extreme precipitation under CO<sub>2</sub> warming. *Clim. Dyn.* **28**, 351–363 (2006).
34. Chen, G., Ming, Y., Singer, N. D. & Lu, J. Testing the Clausius–Clapeyron constraint on the aerosol-induced changes in mean and extreme precipitation. *Geophys. Res. Lett.* **38**, L04807 (2011).
35. Sillmann, J., Kharin, V. V., Zwiers, F. W., Zhang, X. & Bronaugh, D. Climate extremes indices in the CMIP5 multimodel ensemble: Part 2. Future climate projections. *J. Geophys. Res.* **118**, 2473–2493 (2013).
36. Caesar, J. & Lowe, J. A. Comparing the impacts of mitigation versus non-intervention scenarios on future temperature and precipitation extremes in the HadGEM2 climate model. *J. Geophys. Res.* **117**, D15109 (2012).
37. Frieler, K., Meinshausen, M., Schneider von Deimling, T., Andrews, T. & Forster, P. Changes in global-mean precipitation in response to warming, greenhouse gas forcing and black carbon. *Geophys. Res. Lett.* **38**, L04702 (2011).
38. Pendergrass, A. G. & Hartmann, D. L. Global-mean precipitation and black carbon in AR4 simulations. *Geophys. Res. Lett.* **39**, L01703 (2012).
39. Pendergrass, A. G., Lehner, F., Sanderson, B. M. & Xu, Y. Does extreme precipitation intensity depend on the emissions scenario? *Geophys. Res. Lett.* **42**, 8767–8774 (2015).
40. Lin, L., Wang, Z., Xu, Y. & Fu, Q. Sensitivity of precipitation extremes to radiative forcing of greenhouse gases and aerosols. *Geophys. Res. Lett.* **43**, 9860–9868 (2016).
41. Wang, Z. et al. Scenario dependence of future changes in climate extremes under 1.5 and 2 °C global warming. *Sci. Rep.* **7**, 46432 (2017).
42. Sillmann, J., Stjern, C. W., Myhre, G. & Forster, P. M. Slow and fast responses of mean and extreme precipitation to different forcing in CMIP5 simulations. *Geophys. Res. Lett.* **44**, 6383–6390 (2017).
43. Myhre, G. et al. PDRMIP: a precipitation driver and response model inter-comparison project—protocol and preliminary results. *Bull. Am. Meteorol. Soc.* **98**, 1185–1198 (2017).
44. Myhre, G. et al. Radiative forcing of the direct aerosol effect from AeroCom Phase II simulations. *Atmos. Chem. Phys.* **13**, 1–25 (2013).
45. Samset, B. H. et al. Black carbon vertical profiles strongly affect its radiative forcing uncertainty. *Atmos. Chem. Phys.* **13**, 2423–2434 (2013).
46. Boucher, O. et al. Clouds and aerosols. (eds Stocker, T. F., Qin, D., Plattner, G.-K., Tignor, M., Allen, S. K., Boschung, J., Nauels, A., Xia, Y., Bex, V. & Midgley, P. M.) Climate Change 2013: The Physical Science Basis. Contribution of Working Group I to the Fifth Assessment Report of the Intergovernmental Panel on Climate Change (Cambridge University Press, Cambridge, United Kingdom and New York, NY, USA, 2013).
47. Samset, B. H. et al. Weak hydrological sensitivity to temperature change over land, independent of climate forcing. *npj Clim. Atmos. Sci.* **1**, 20173 (2018).
48. Ocko, I. B., Ramaswamy, V. & Ming, Y. Contrasting climate responses to the scattering and absorbing features of anthropogenic aerosol forcings. *J. Clim.* **27**, 5329–5345 (2014).
49. Abdul-Razzak, H. & Ghan, S. J. A parameterization of aerosol activation: 2. Multiple aerosol types. *J. Geophys. Res.* **105**, 6837–6844 (2000).



**Open Access** This article is licensed under a Creative Commons Attribution 4.0 International License, which permits use, sharing, adaptation, distribution and reproduction in any medium or format, as long as you give appropriate credit to the original author(s) and the source, provide a link to the Creative Commons license, and indicate if changes were made. The images or other third party material in this article are included in the article's Creative Commons license, unless indicated otherwise in a credit line to the material. If material is not included in the article's Creative Commons license and your intended use is not permitted by statutory regulation or exceeds the permitted use, you will need to obtain permission directly from the copyright holder. To view a copy of this license, visit <http://creativecommons.org/licenses/by/4.0/>.

© The Author(s) 2019